

Complex tribomechanical characterization of ZnO nanowires: nanomanipulations supported by FEM simulations

Sergei Vlassov¹, Boris Polyakov², Sven Oras¹, Mikk Vahtrus¹, Mikk Antsov¹, Andris Šutka^{1,3}, Krisjanis Smits², Leonid M Dorogin⁴ and Rünno Lõhmus¹

¹Institute of Physics, University of Tartu, Ravila 14c, 50412, Tartu, Estonia

²Institute of Solid State Physics, University of Latvia, Kengaraga 8, LV-1063, Riga, Latvia

³Institute of Silicate Materials, Riga Technical University, Paula Valdena 03/7, LV-1048, Riga, Latvia

⁴Peter Grünberg Institute and Institute for Advanced Simulation, Forschungszentrum Jülich GmbH, Wilhelm-Johnen-Straße, 52428 Jülich, Germany

E-mail: l.dorogin@fz-juelich.de

Received 17 March 2016, revised 30 May 2016


Accepted for publication 7 June 2016

Published 4 July 2016



Abstract

In the present work, we demonstrate a novel approach to nanotribological measurements based on the bending manipulation of hexagonal ZnO nanowires (NWs) in an adjustable half-suspended configuration inside a scanning electron microscope. A pick-and-place manipulation technique was used to control the length of the adhered part of each suspended NW. Static and kinetic friction were found by a ‘self-sensing’ approach based on the strain profile of the elastically bent NW during manipulation and its Young’s modulus, which was separately measured in a three-point bending test with an atomic force microscope. The calculation of static friction from the most bent state was completely reconsidered and a novel more realistic crack-based model was proposed. It was demonstrated that, in contrast to assumptions made in previously published models, interfacial stresses in statically bent NW are highly localized and interfacial strength is comparable to the bending strength of NW measured in respective bending tests.

 Online supplementary data available from stacks.iop.org/NANO/27/335701/mmedia

Keywords: friction, manipulation, ZnO, nanowires, strength, Young’s modulus

(Some figures may appear in colour only in the online journal)

1. Introduction

Nanowires (NWs) are among the most important objects in modern science and have a number of promising applications in nanotechnology [1–4]. Plenty of prototype nanoelectromechanical systems (NEMS) based on NWs have already been demonstrated during the last few decades [5]. The fabrication and functioning of NW-based devices are tightly related to tribomechanical problems since they often involve the relative motion and mechanical interaction between a NW and other components. The situation is complicated by the fact that the behaviour of nanostructures differs significantly

from their macroscopic analogues. In particular, NWs are typically much stronger and more flexible compared to their bulk counterparts [6]. Interfacial phenomena is another issue of great importance for nanoscale systems. For example, adhesion and static friction are often high enough to hold a bent NW on a flat surface in a bent state without gluing or welding [7]. Such a strong adhesion can be beneficial for the fastening of individual components of a nanoscale system. On the other hand, strong adhesion can hinder the normal functioning of devices like relays and switches. Moreover, adhesion and friction may depend on time [8]. Therefore, deeper understanding and control over the mechanical and

tribological properties of the nanoscale systems are of great importance for the successful implementation of NEMS.

Manipulation of individual nanostructures is one of the most common methods for studying the mechanical and tribological properties at the nano and atomic scales. There are several techniques widely used for the mechanical characterization of individual NWs, including nanoindentation [9–11], the three-point bending test [12–14], the cantilever beam bending test [6, 15], the tensile test [16, 17], or the mechanical resonance method [18, 19]. Since nanomechanical characterization became a common practice, mechanical properties of many nanoscale materials can be found in the literature (however, it is fair to say that the reported values often vary drastically from author to author). The tribological properties of nanoscale systems are significantly less studied. Most of the works in this field are performed with different spherical or faceted nanoparticles manipulated with an atomic force microscope (AFM) [20–22] or inside a scanning electron microscope (SEM) [23]. The force during manipulation is typically linked to friction forces and can be detected via dissipated power, torsional deflection of the cantilever or an external force sensor.

In recent years, nanotribological experiments have also been carried out on NW-based systems [24–33]. NWs feature a number of benefits in comparison to nanoparticles for enriching the experimental methodology toolkit. Namely, having one dimension outside the nanoscale, NW enables relatively easy location (NWs may be visible even in an optical microscope) and manipulation (dragging, pulling, bending, etc). Recently, manipulation has been employed for experimental [34] and theoretical [35] studies of the rotational friction of elongated nanostructures. Moreover, in contrast to the manipulation of nanoparticles, the use of elastic NW for nanotribological experiments can eliminate the need to use external force sensors. The profile of the NW during the manipulation on a substrate is determined by the interplay between the elastic forces inside the NW and the interaction forces between the NW and substrate. Therefore, given that the geometry and elastic properties of a NW are known, the NW can serve as a self-sensing system and frictional forces can be extracted by observing the NW profile during manipulation. The basic principles of the self-sensing approach were demonstrated in a simplified form by Bordag *et al* [24], Conache *et al* [25, 26], Stan *et al* [27] and Strus *et al* [28] in AFM-based experiments. Later, the self-sensing method was elaborated further by introducing improved analytical models by Dorogin *et al* [29, 30], Polyakov *et al* [31], Antsov *et al* [7] and recently by other authors [32, 33].

As was shown in the listed works, the self-sensing approach can be combined with different regimes of manipulation, and enables us to calculate kinetic, static and distributed friction forces. In particular, kinetic friction can be measured by observing the curvature of the NW dragged at its midpoint with an AFM tip [29–31, 36]. Static friction can be measured by bending a NW from one end, while part of the NW stays immobile due to adhesion on the substrate. The profile of the NW in the most bent state before displacement

of the adhered part is used to extract the static friction value [29, 30, 37].

In the present work, we had advanced the self-sensing approach by introducing a half-suspended NW configuration in combination with a pick-and-place manipulation, which enabled us to control the position and length of the adhered part of each NW. Experiments were performed inside a high resolution SEM on hexagonal ZnO NWs positioned over the trenches etched in a Si substrate and included measurements of the bending strength, static and kinetic friction. For the first time, kinetic friction was measured in the rotation regime. The calculation of static friction from the most bent state and the stress distributions in manipulated NWs were completely reconsidered. The new more realistic model was inspired by the concepts of fracture mechanics making use of finite element method (FEM) computations.

2. Materials and methods

2.1. Method

All types of measurements considered in the present study required the NW to be located partly suspended over the trench made in a flat substrate. Depending on whether one of the NW's ends is freely suspended or not, two configurations are possible: the three-point bending scheme (figure 1(a)) and the cantilever beam bending scheme (figure 1(b)).

All tribological and strength measurements were performed on cantilevered NWs (first scheme) inside a high-resolution SEM (HRSEM, Helios Nanolab 600, FEI, spatial resolution approx. 1 nm), using a polar coordinate nanomanipulator (MM3A-EM, Kleindiek) equipped with an AFM probe (ATEC-CONT, Nanosensor). Video data were recorded during measurements, providing real-time visual feedback on the behavior of the loaded NW, the actual contact point between the probe and NW at every stage of the manipulation, the corresponding profile of the manipulated NW, and the events of NW displacement.

Young's modulus for the 'self-sensing' in tribological tests was measured by an AFM (Dimension Edge, Bruker) in a 3-point bending configuration using tapping mode cantilevers (PPP-NCHR, Nanosensors) with normal force constant between $50 \pm 2.5 \text{ N m}^{-1}$. Normal force constant for each cantilever was calculated using the geometry of the cantilever measured by HR-SEM [38]. To extract static friction data, experimental conditions were simulated with FEM using COMSOL Multiphysics 5 software. Structural characterization of ZnO NWs was performed with a high-resolution transmission electron microscope (HRTEM, Tecnai GF20, FEI).

2.2. ZnO NWs

ZnO NWs were chosen due to their physical properties, geometry and a number of promising applications [39]. ZnO NWs can withstand significant bending deformations without

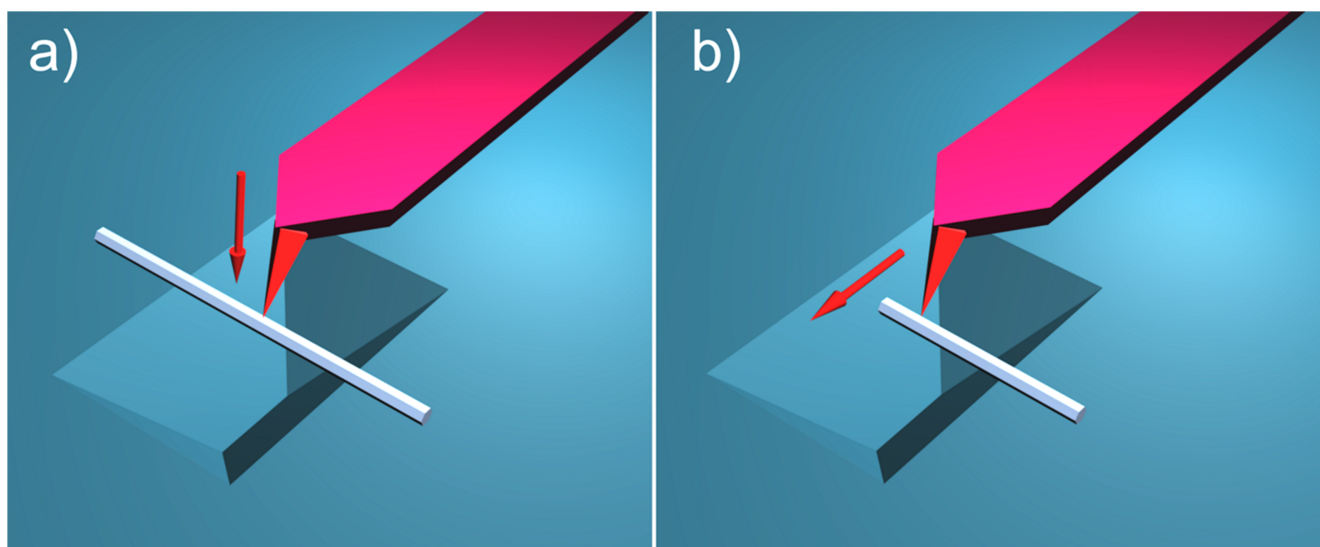


Figure 1. (a) Schematics of the 3-point bending test with AFM and (b) cantilever beam bending test inside SEM. Note that the lateral sizes of the AFM cantilever, NW and grooves are not scaled proportionally for better visual perception of the experiment schematics.

fracture [30]. In addition, ZnO NWs can be synthesized with a well-pronounced hexagonal cross-section [40].

ZnO NWs were synthesized using the solvothermal synthesis process [41]: 15 ml of 0.1 M zinc acetate dehydrate ($\text{Zn}(\text{CH}_3\text{CO}_2)_2 \cdot 2\text{H}_2\text{O}$) (98%, Sigma Aldrich) and 30 ml of 0.5 M NaOH (98%, Sigma Aldrich) solution in ethanol (99%, Merk) were prepared separately by dissolving precursors at 80 °C under vigorous stirring. After dissolving, both solutions were mixed together and left for stirring at 80 °C for the next 10 h. In the next step, the mixture was transferred into a Teflon-lined stainless steel autoclave of 50 ml capacity, sealed and heated at 150 °C for 24 h. For structural characterization, the obtained NWs were filtered and washed with methanol and water several times.

2.3. Preparation of the substrates

A p-type Si wafer (0.001–0.004 Ω cm, (1 0 0) crystal orientation) was used as the substrate. A drop of a polystyrene (PS) spheres suspension (PS latex 900 nm) was placed on the substrate. After the evaporation of the solvent, the silicon substrate with the PS spheres was heated to 110 °C, which is higher than the glass transition point ($T_g \sim 93$ °C) of PS, to fix the PS sphere mask onto the silicon substrate and to melt the adjacent PS spheres together. Then anodization was proceeded at a constant voltage of 20 V in 0.3 M oxalic acid for 3–5 s. After anodization, the PS spheres used as an initial mask were removed by immersion in toluene. To etch the exposed Si surface, anodized Si specimens were immersed for 1–2 min in 25% tetramethyl ammonium hydroxide at 90 °C, and then the sample was immersed in concentrated HF to remove the remaining SiO_2 mask. This procedure resulted in the formation of inverted pyramids of different sizes (figure 2).

ZnO NWs were deposited from the solution by drop casting. Prior to the experiments the substrates were annealed

to 200 °C for 30 min to remove any possible organic contaminants.

3. Results and discussion

3.1. Structural characterization

According to the SEM images, the diameters of ZnO NWs ranged from a few tens to a few hundreds of nm, while lengths ranged from several hundred nm to a few microns. Close-up inspection revealed a well-pronounced hexagonal cross-section characteristic to wurtzite group structures (figures 3(a), (b)). A perfect monocrystalline structure is seen in the HRTEM images (figure 3(d)). The measured interplanar distance is about 2.7 Å, which is close to 2.8 Å measured in [42], and corresponds to the (01 $\bar{1}$ 0) planes of hexagonal wurtzite ZnO. The direction of the (01 $\bar{1}$ 0) planes of hexagonal wurtzite ZnO are perpendicular to the axis of the NW, indicating that $\langle 0001 \rangle$ is the preferred growth direction of the ZnO NW.

3.2. Young's modulus measurement (3-point beam bending test)

Tribological measurements considered in the present work assume a known Young's modulus (E). Mechanical properties of ZnO NWs can easily be found in the literature [18, 43–53]. However, the reported values of the Young's modulus scatter drastically, ranging from a few tens, e.g. [43, 44, 50, 51] to hundreds of GPa, e.g. [45, 48, 52]. Moreover, some investigations clearly demonstrate the dependence of elastic properties on the NW diameter, e.g. [45, 47, 48, 53], while others do not, e.g. [18, 46]. Therefore, it is evident that the mechanical characterization should be performed for every particular set of NWs used in the manipulation experiments.

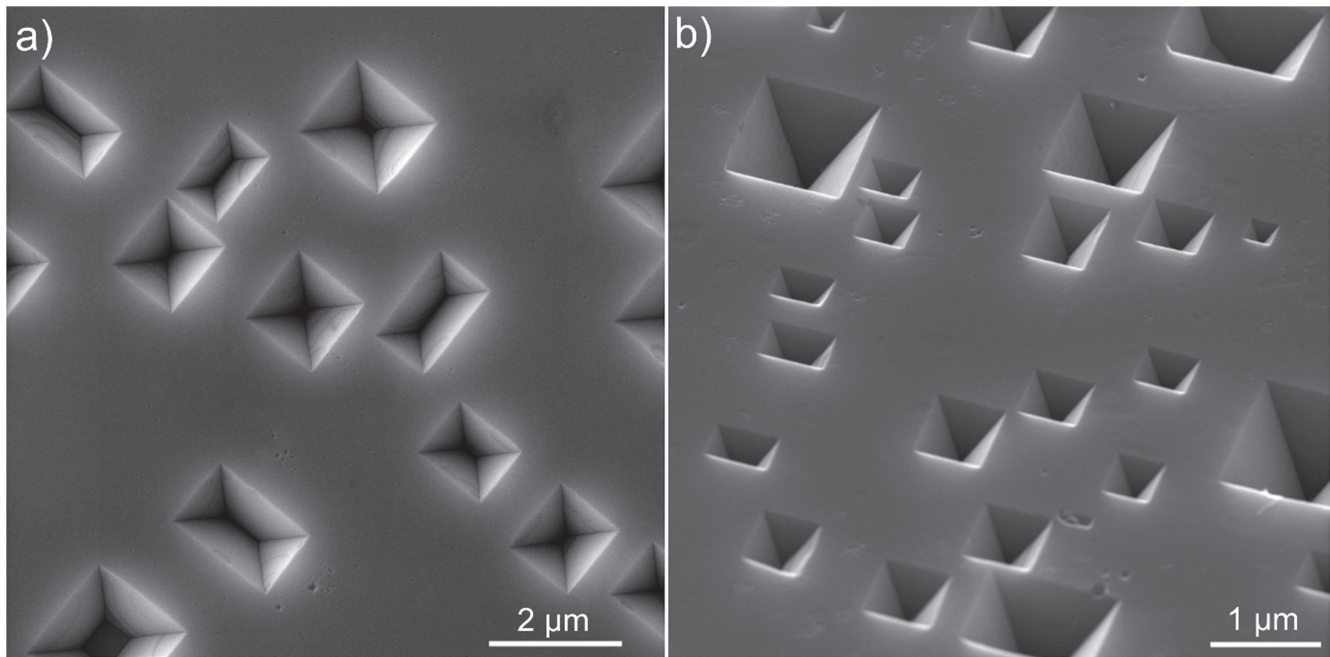


Figure 2. SEM image of inverted pyramids etched in the Si wafer. The image is taken under 45 degrees tilt.

Young's moduli of NWs used in the present study were measured by an AFM-based 3-point bending test (figure S1 in the electronic supplementary information) as one of the most reliable techniques for the mechanical characterization of one-dimensional nanostructures as follows [54]:

$$E = \frac{(FL^3)}{8d(Ad^2 + 24I)}, \quad (1)$$

where F is the force acting on the NW, L the length of the suspended part of NW, d the deflection of the center point, A the area of the cross-section and I the area moment of inertia. The results of the measurements for 21 ZnO NWs of different diameters are plotted in figure 4.

A clear size effect can be seen for NW diameters below 40 nm. Measured values are higher than those reported in the majority of papers dedicated to the elastic properties of ZnO NWs. On the other hand, our results are more consistent with the bulk value of 140 GPa for ZnO and are in a good agreement with those reported by Chen *et al* [45] and Stan *et al* [48]. However, in contrast to [45], the size effect in our case appears at smaller diameters.

Typically, elastic stiffening of NWs with a decrease of diameter is attributed mainly to the increased contribution of surface effects for nanostructures like, e.g. surface bond saturation resulting from an increased electron density [55] or a decrease in surface interatomic spacing due to surface reconstruction [56, 57]. Since the scope of the present work is related mainly to tribological measurements, and the Young's modulus is just one of the parameters needed for the extraction of frictional data in the self-sensing approach, we will leave detailed discussion of the measured Young moduli values outside the paper.

3.3. Cantilever beam bending tests

Competition between the NW/substrate contact strength and inner NW strength during the bending test leads to either fracture or displacement of the NW. Displacement of most of the NWs from their initial locations as deposited from the solution was impossible, most probably due to the contact ageing [58]. Contact ageing is a common observation of increasing friction with time of undisturbed nanocontact [59, 60]. The exact nature of contact ageing in this case is not clear yet. Moreover, the adhered part of the NWs was typically too long for convenient manipulations. It was conditioned by the deposition from the solution: NWs preferred to be situated either between or inside the trenches. To make tribological testing possible and assure fresh contacts, the 'pick-and-place' approach was applied by breaking the suspended part and transferring it to a suitable place in the vacuum conditions of the SEM chamber (figures 5(a)–(e)). This also enabled us to control the length of the adhered part.

3.3.1. Bending strength. For the NWs broken in the bending test, bending strength σ_{st} was calculated as the maximum stress in a NW before fracture $\sigma_{st} = E \cdot d \cdot |\kappa|/2$, where κ is the curvature at which the bent beam is fractured or displaced, E is the Young's modulus and d is the diameter of NW [61]. Since the Young's modulus of our ZnO NWs was found to depend on diameter, we could not use one single E value for the calculation of forces involved in the bending test, but needed to estimate its value on the basis of the dependence (figure 4) obtained in the 3-point bending test.

Figure 6 represents the bending strength calculated for 59 broken NWs (blue circles). It can be seen that both average strength and data scattering increase as diameter decreases. Numerical values of the strength are close to the theoretical

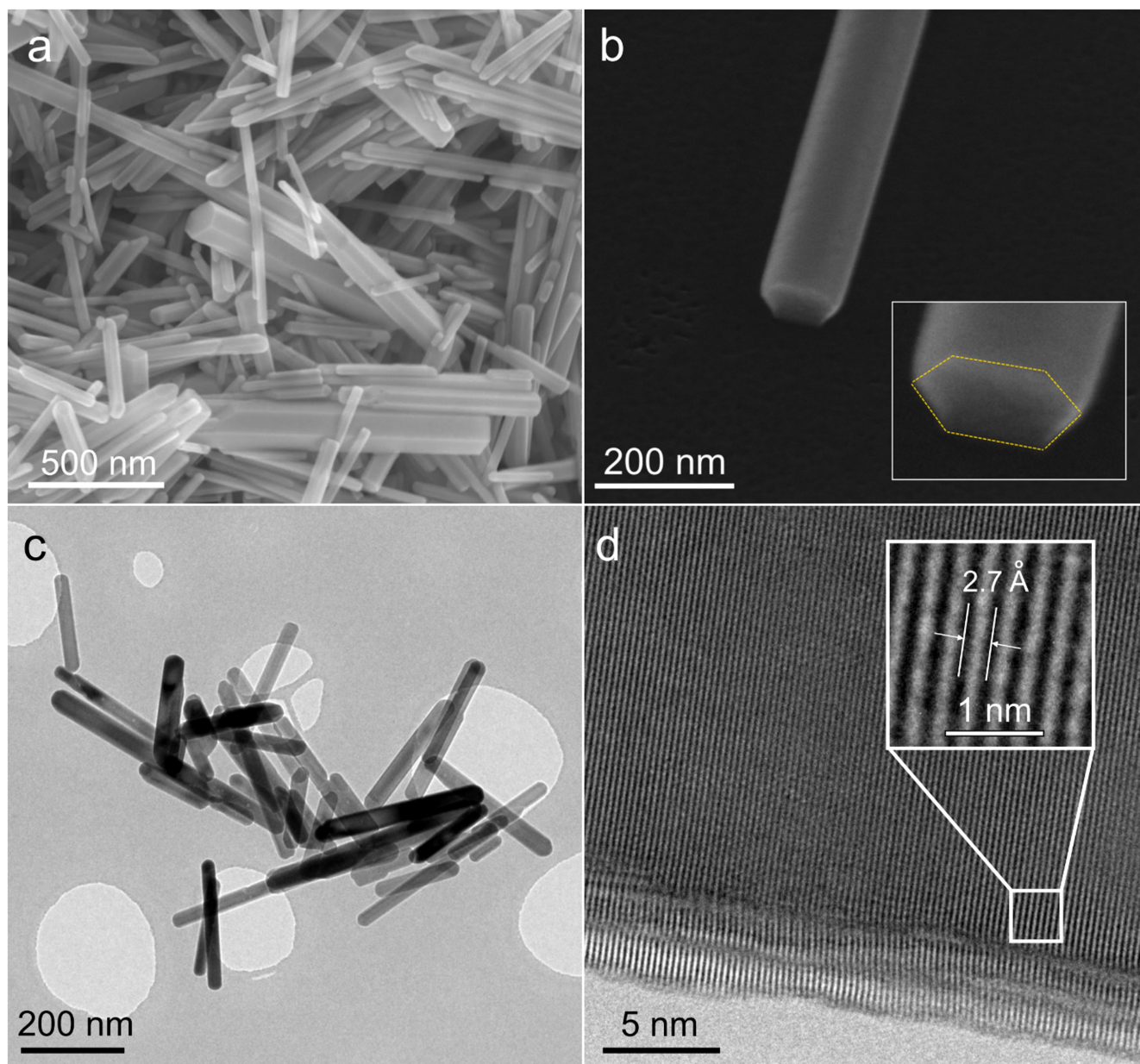


Figure 3. SEM (a), (b) and TEM (c), (d) images of ZnO NWs.

strength, which can be estimated as $E/10$ based on the atomic bonding consideration [62, 63]. For convenience, $E/10$ values are plotted on the same graph (figure 6, red triangles). Such high strength indicates that the ZnO NWs are of the highest quality, with a low concentration of the major structural defects.

Scattering of the strength values is a common phenomenon for NWs [64, 65], especially in cantilever beam configuration where stress distribution is highly nonuniform. The strength of NW in the bending test is determined by the presence of a critical defect [66] in the vicinity of the maximal strain in the deformed material. NWs used in our experiment are of high quality, which can be concluded both from electron microscopy images and from high strength values, therefore an increase of strength data scattering with a decrease of NW diameters is expected.

3.3.2. Static friction. After the picked NW was positioned into a desired location on the substrate, static friction was measured. Static friction, however, is known to be strongly time dependent due to the contact aging [67]. The systematic and detailed study of contact aging is outside the scope of the present paper, therefore we focused on the static friction of fresh contacts. Each experiment started with the positioning of the NW broken in the bending test into a desired location. Then, prior to the real measurements, NW was displaced in order to ‘reset’ the static friction to its minimal value and then immediately was bent and displaced again to measure the fresh static friction.

Similar to the strength measurements, the calculation of static friction from the bending experiment relied on the profile of the NW in the most bent state prior to the displacement of the adhered part (figure 5(f)). In previous

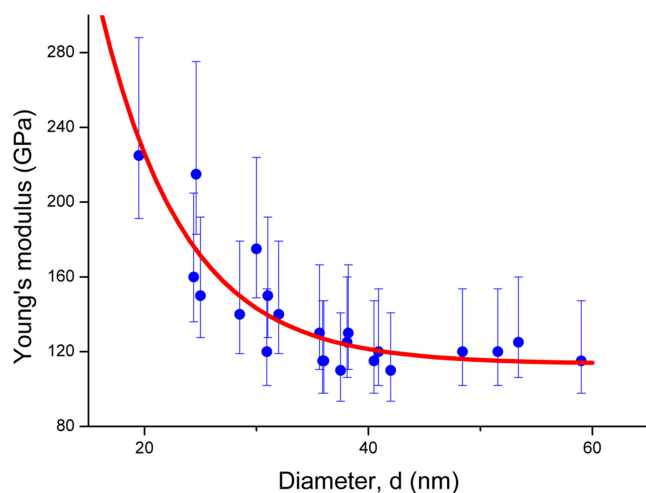


Figure 4. Young's modulus E measured for 21 ZnO NWs of different diameters d , plotted with blue and exponential interpolation fit lined in red.

works dedicated to the calculation of static friction from the 'most bent state', interfacial stresses and the corresponding friction force were assumed to be linearly distributed in the adhered part [29, 30]. In this work, we performed FEM simulations for all NWs that were bent and displaced in the experiment in order to examine the stress distributions in the NW/substrate interface more accurately. ZnO NW was modelled as a prismatic elastic beam with a hexagonal cross-section. Part of the beam was rigidly fixed to simulate the NW/substrate contact in a static situation when NW is loaded from one end, but the adhered part is immobile. Geometrical parameters of the wire, the length of the adhered part, maximal deflection, as well as the point of external force applied to the wire were taken directly from the corresponding experiment. Values of Young's modulus were chosen separately for every particular experiment based on the NW diameter in accordance with the AFM measurements, as depicted in figure 4. A more detailed technical description of the FEM simulations can be found in the electronic supplementary information.

Results of the FEM simulations revealed a strong deviation from linearly distributed stress. According to the FEM model, the forces in contact between an elastically bent NW and a substrate are highly non-uniform and most of the interfacial shear stress is concentrated in close vicinity to the interface between the adhered and suspended part of the NW (figure 7). Therefore, it is more reasonable to consider the overcoming of the static friction as a crack instability problem in the NW/substrate interface at the point of maximal interfacial stress. As soon as a crack forms, it will propagate without additional force and the whole NW will be displaced. Static friction can be represented then in terms of the maximal interfacial shear strength just before displacement of the whole NW. It is evident that in this case, static friction will be significantly higher than previous models predict. Indeed, when we calculated the maximal shear stress for the case depicted in figure 7 using the simplified approach as

described in [30], we obtained 31 MPa in contrast to 1.8 GPa calculated with our FEM model. In total, the median value of the maximal interfacial shear strength of the fresh contact (second displacement) calculated using the FEM model for 16 'bend-and-displace' tests was found to be 1.3 ± 0.7 GPa, which is comparable with the bending strength of ZnO NWs.

High values obtained with the new model may seem doubtful at first. However, the validity of the new model is strongly supported by experimental observations.

First, curvatures of the NWs in both strength and static friction tests are also comparable. It means that breaking the NW/substrate contact and breaking the NW itself are indeed two competitive processes and should have comparable values.

Second, in the new model, static friction does not depend on the length of the adhered part and this was clearly demonstrated experimentally. We succeeded to displace one NW from its initial position without breaking. It means that the strength of this particular NW was higher than the strength of the aged contact. The adhered part of this NW was relatively long and we observed a stepwise displacement (figure 8). When the shear strength in the bending test was exceeded, some fraction of the adhered part released, but NW was still held on the substrate by the shorter part. The tip was moving smoothly at a constant velocity; nevertheless, transitions between different adhered states were abrupt, enabling five separate calculations of shear strength for each adhered state. Every time, displacement happened at a similar maximal curvature of the NW. According to the FEM model, shear strengths in these points were 5.7/6.6/6.9/5.7/5.1 GPa.

Third, a substantial difference between static and kinetic friction was also observed for other nanoscale systems using completely different methods [23, 34].

3.3.3. Kinetic friction. In some cases after overcoming the static friction in the bending test, the NW did not straighten completely, but continued to rotate while preserving the bent profile of a constant curvature (figures 5(g), (h)). Such behavior allowed us to estimate the kinetic friction involved in rotation. Since the rotating part was moving as a rigid object with a constant profile, kinetic friction can be parameterized simply as an average interfacial shear strength which is the force acting on the NW divided by the contact area (area of the bottom facet of the NW contacting the substrate) $\tau = F/A$. The total force can be found from the profile of the bent NW during the rotational motion. The calculated friction data are highly scattered (figure 9). For most of the NWs, friction values were below 15 MPa; however, in some cases friction was significantly higher, reaching tens of MPa. Some NWs rotated at very small bending curvatures, making it impossible to accurately calculate friction by mathematical fitting. Such cases are denoted on the histogram as $\ll 1$. In general, obtained values correlate well with a few MPa as found for the ZnO/Si system by other methods. Average shear stresses obtained by

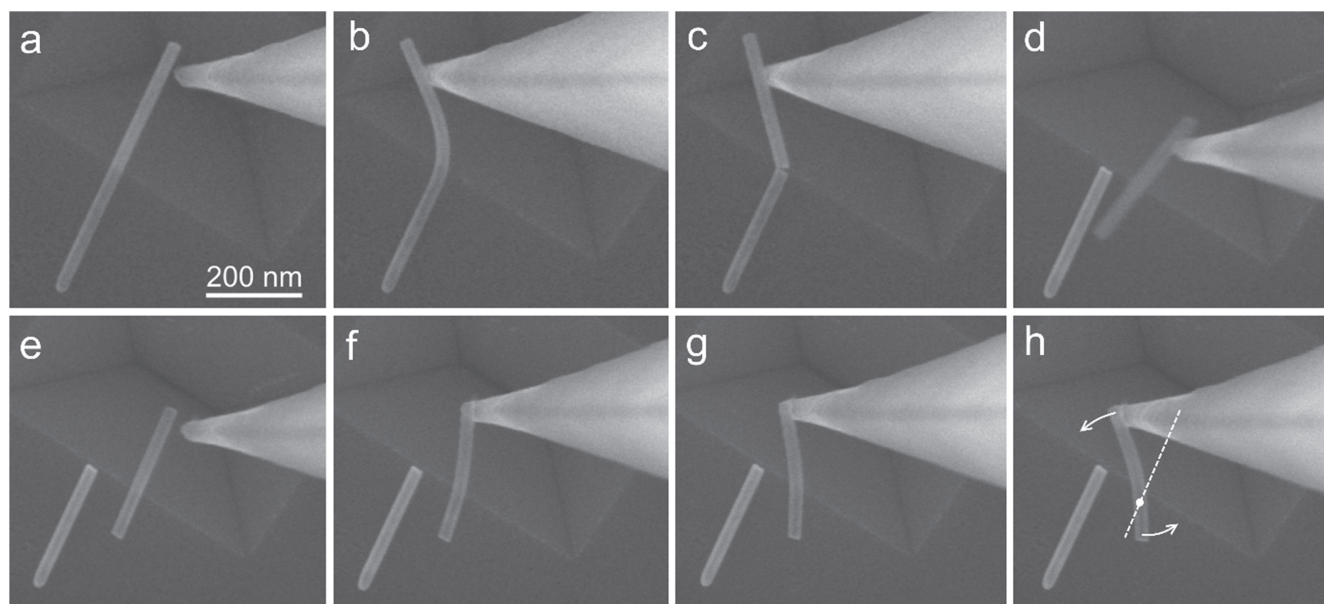


Figure 5. Typical manipulation of half-suspended ZnO NW inside HRSEM: (a)–(c) bending and breaking of the NW, (d)–(e) pick-and-place manipulation, (f)–(g) static friction measurements, (g)–(h) bent NW is rotating.

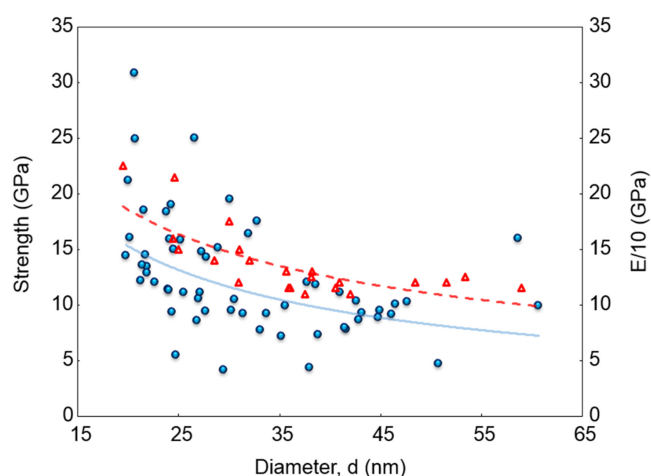


Figure 6. Bending strength (blue circles) and $E/10$ (red triangles) plotted versus diameter d of NW. Second power trend lines are fitted with respective colours for convenience.

dragging ZnO NWs on a Si wafer in its midpoint were found to be 2.1 MPa [48] and 3.2 MPa [31], and 1 MPa in a pulling experiment [68].

The high scattering of kinetic friction values is common for nanowire-on-substrate systems [25]. Scattering of kinetic friction values is mainly related to local asperities, surface defects and other imperfections both on the substrate and on NWs. Due to the short range of van der Waals interaction, the presence of a few or even single asperity is able to decrease real NW-substrate contact by an order of magnitude, and correspondingly decrease friction [58]. On the TEM image (figure 3(d)) of the ZnO NW it is seen that the NW surface is not perfectly smooth, but has some imperfections that can vary from NW to NW. According to the AFM measurements, the root mean squared roughness (RMS) of the structured Si substrate is 0.3 nm, which is rather flat, but not sufficient to equalize real and apparent contact areas

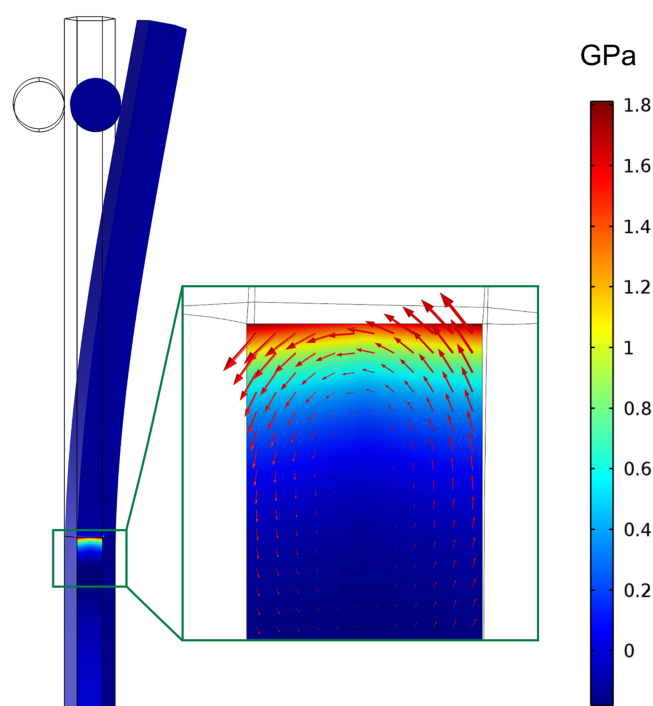


Figure 7. Interfacial stress distribution in the facet of elastically bent ZnO NW contacting the Si substrate modeled with FEM. The model is static and deflection corresponds to the most bent state before displacement of the adhered part in the real bending test. Arrows indicate the direction and relative magnitude of the interfacial forces at each point (for convenience, the density of the arrows decreased in comparison to the real number of elements in the FEM model).

(for comparison the RMS value for atomically flat silicon is approximately 0.04 (HOPG 0.03 [69])). Although for fundamental studies of friction at the atomic scale smoother substrates can be beneficial, our system corresponds well to the real NEMS applications with similar materials and surface treatment

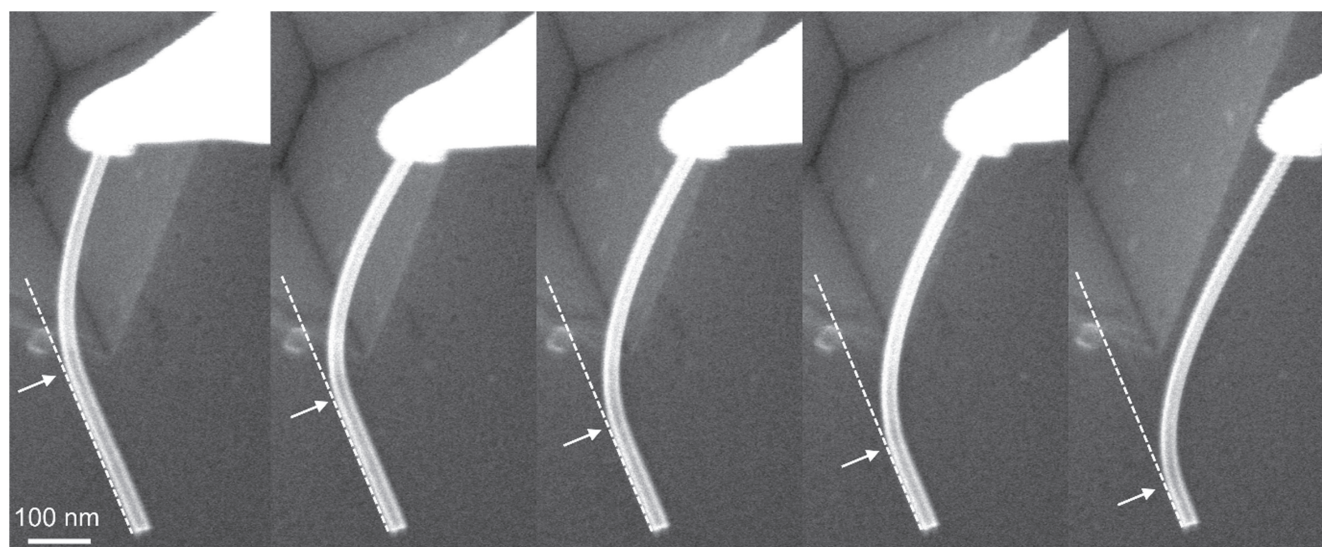


Figure 8. Stepwise displacement of adhered NW. Arrows indicate the point that separates the moving part of the NW from the part rigidly adhered to the substrate.

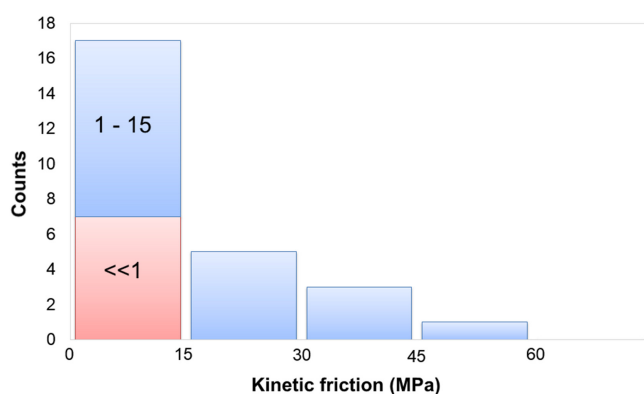


Figure 9. Statistical distribution of kinetic friction from rotation observations of suspended ZnO NWs.

techniques. Another issue that is worth noting is that the velocity factor was not taken into account when calculating the kinetic friction in the rotational experiment. Moreover, the situation is complicated since different parts of the NW move at different velocities. Previously, it was demonstrated by different authors that friction can be slightly dependent on velocity in the wide range of velocities [70–72]. In our experiments, the tip is always moving at the constant velocity of approximately 100 nm s^{-1} . However, since the length of both the suspended and adhered parts varied from experiment to experiment, the real velocity of the ZnO NW relative to the substrate also varied and could have a minor contribution in data scattering.

4. Conclusions

In this work, we carried out tribomechanical studies of ZnO NWs in a half-suspended configuration. Measurements consisted in bending and displacing half-suspended NWs with subsequent analysis of the NW bending strain profile during manipulation without any external force detection. A more realistic model based on the FEM simulations was created for the extraction of

the static friction from the manipulation data. The previous ‘linear’ model might severely underestimate stresses generated at the NW/substrate interface, and the difference increases for the longer adhered part. It was shown that interfacial shear strengths of the ZnO-NW/Si-substrate system is comparable to the bending strength of ZnO NWs. Kinetic friction was measured in rotational experiments and the obtained values correlate well with results measured for the ZnO/Si system by other methods. On the basis of the present study, it can be concluded that the manipulation of suspended NWs have a number of strong advantages for nanotribological studies in comparison to manipulations on a flat substrate. A suspended configuration in combination with the pick-and-place technique allows us to perform multiple measurements on the same NW with a precisely varied contact area. Moreover, a suspended configuration enables us to avoid the tip wear caused by the tip/substrate contact, therefore assuring longer tip lifetime.

Acknowledgments

This work was supported by the Institutional Research Funding project IUT2-25 ‘Structure sensitive interaction mechanisms in functional materials at nanoscale’, COST Action MP1303 and International Research Laboratory Initiative of ITMO University. The authors are grateful to Prof Bo Persson for the useful discussion in the friction analysis part.

References

- [1] Lu W and Lieber C M 2006 Semiconductor nanowires *J. Phys. D: Appl. Phys.* **39** R387–406
- [2] Xia Y, Yang P, Sun Y, Wu Y, Mayers B, Gates B, Yin Y, Kim F and Yan H 2003 One-dimensional nanostructures: synthesis, characterization, and applications *Adv. Mater.* **15** 353–89

- [3] Tian Y, Bakaul S R and Wu T 2012 Oxide nanowires for spintronics: materials and devices *Nanoscale* **4** 1529–40
- [4] Zhang Q, Yodyingyong S, Xi J, Myers D and Cao G 2012 Oxide nanowires for solar cell applications *Nanoscale* **4** 1436–45
- [5] Lee S K, Choi H J, Pauzaskie P, Yang P, Cho N K, Park H-D, Suh E K, Lim K Y and Lee H J 2004 Gallium nitride nanowires with a metal initiated metal-organic chemical vapor deposition (MOCVD) approach *Phys. Status Solidi b* **1** 2775–8
- [6] Vlassov S, Polyakov B, Dorogin L M, Antsov M, Mets M, Umalas M, Saar R, Löhms R and Kink I 2014 Elasticity and yield strength of pentagonal silver nanowires: *in situ* bending tests *Mater. Chem. Phys.* **143** 1026–31
- [7] Antsov M, Dorogin L, Vlassov S, Polyakov B, Vahtrus M, Mougou K, Löhms R and Kink I 2014 Analysis of static friction and elastic forces in a nanowire bent on a flat surface: a comparative study *Tribol. Int.* **72** 31–4
- [8] Gitis N and Volp L 1991 Nature of static friction time dependence *J. Phys. D: Appl. Phys.* **25** 605–12
- [9] Li X, Gao H, Murphy C J and Caswell K K 2003 Nanoindentation of silver nanowires *Nano Lett.* **3** 1495–8
- [10] Feng G, Nix W D, Yoon Y and Lee C J 2006 A study of the mechanical properties of nanowires using nanoindentation *J. Appl. Phys.* **99** 0–10
- [11] Sohn Y-S, Park J, Yoon G, Song J, Jee S-W, Lee J-H, Na S, Kwon T and Eom K 2010 Mechanical properties of silicon nanowires *Nanoscale Res. Lett.* **5** 211–6
- [12] Zhou P, Wu C and Li X 2008 Three-point bending Young's modulus of nanowires *Meas. Sci. Technol.* **19** 115703
- [13] Leclerc C, Cornelius T W, Ren Z, Davydok A, Micha J-S, Robach O, Richter G, Belliard L and Thomas O 2015 *In situ* bending of an Au nanowire monitored by micro Laue diffraction *J. Appl. Crystallogr.* **48** 291–6
- [14] Zhang H, Tang J, Zhang L, An B and Qin L-C 2008 Atomic force microscopy measurement of the Young's modulus and hardness of single LaB₆ nanowires *Appl. Phys. Lett.* **92** 173121
- [15] Silva E C C M, Tong L, Yip S and Van Vliet K J 2006 Size effects on the stiffness of silica nanowires *Small* **2** 239–43
- [16] Zhu Y, Qin Q, Xu F, Fan F, Ding Y, Zhang T, Wiley B J and Wang Z L 2012 Size effects on elasticity, yielding, and fracture of silver nanowires: *in situ* experiments *Phys. Rev. B* **85** 1–7
- [17] Li X, Wei X L, Xu T T, Ning Z Y, Shu J P, Wang X Y, Pan D, Zhao J H, Yang T and Chen Q 2014 Nanoindentation of silver nanowires *Appl. Phys. Lett.* **104** 103110
- [18] Bai X D, Gao P X, Wang Z L and Wang E G 2003 Dual-mode mechanical resonance of individual ZnO nanobelts *Appl. Phys. Lett.* **82** 4806–8
- [19] Perisanu S, Gouttenoire V, Vincent P, Ayari A, Choueib M, Bechelany M, Cornu D and Purcell S T 2008 Mechanical properties of SiC nanowires determined by scanning electron and field emission microscopies *Phys. Rev. B* **77** 165434
- [20] Dietzel D, Mönninghoff T, Jansen L, Fuchs H, Ritter C, Schwarz U D and Schirmeisen A 2007 Interfacial friction obtained by lateral manipulation of nanoparticles using atomic force microscopy techniques *J. Appl. Phys.* **102** 12–7
- [21] Dietzel D, Ritter C, Mönninghoff T, Fuchs H, Schirmeisen A and Schwarz U D 2008 Frictional duality observed during nanoparticle sliding *Phys. Rev. Lett.* **101** 125505
- [22] Nita P, Casado S, Dietzel D, Schirmeisen A and Gnecco E 2013 Spinning and translational motion of Sb nanoislands manipulated on MoS₂ *Nanotechnology* **24** 325302
- [23] Polyakov B, Vlassov S, Dorogin L, Butikova J, Antsov M, Oras S and Lohmus R 2014 Manipulation of nanoparticles of different shapes inside a scanning electron microscope *Beilstein J. Nanotechnol.* **5** 133–40
- [24] Bordag M, Ribayrol A, Conache G, Fröberg L E, Gray S, Samuelson L, Montelius L and Pettersson H 2007 Shear stress measurements on InAs nanowires by AFM manipulation *Small* **3** 1398–401
- [25] Conache G, Gray S M, Ribayrol A, Fröberg L E, Samuelson L, Pettersson H and Montelius L 2009 Friction measurements of InAs nanowires on silicon nitride by AFM manipulation *Small* **5** 203–7
- [26] Conache G, Gray S M, Ribayrol A, Fröberg L E, Samuelson L, Montelius L and Pettersson H 2010 Comparative friction measurements of InAs nanowires on three substrates *J. Appl. Phys.* **108** 094307
- [27] Stan G, Krylyuk S, Davydov A V and Cook R F 2011 Bending manipulation and measurements of fracture strength of silicon and oxidized silicon nanowires by atomic force microscopy *J. Mater. Res.* **27** 562–70
- [28] Strus M C, Lahiji R R, Ares P, López V, Raman A and Reifenger R 2009 Strain energy and lateral friction force distributions of carbon nanotubes manipulated into shapes by atomic force microscopy *Nanotechnology* **20** 385709
- [29] Dorogin L M, Polyakov B, Petruhins A, Vlassov S, Löhms R, Kink I and Romanov A E 2012 Modeling of kinetic and static friction between an elastically bent nanowire and a flat surface *J. Mater. Res.* **27** 580–5
- [30] Dorogin L M, Vlassov S, Polyakov B, Antsov M, Löhms R, Kink I and Romanov A E 2013 Real-time manipulation of ZnO nanowires on a flat surface employed for tribological measurements: experimental methods and modeling *Phys. Status Solidi* **250** 305–17
- [31] Polyakov B, Dorogin L M, Löhms A, Romanov A E and Löhms R 2012 *In situ* measurement of the kinetic friction of ZnO nanowires inside a scanning electron microscope *Appl. Surf. Sci.* **258** 3227–31
- [32] Hou L, Wang S and Huang H 2015 A simple criterion for determining the static friction force between nanowires and flat substrates using the most-bent-state method *Nanotechnology* **26** 165702
- [33] Xie H, Wang S and Huang H 2015 Kinetic and static friction between alumina nanowires and a Si substrate characterized using a bending manipulation method *J. Mater. Res.* **30** 1852–60
- [34] Polyakov B, Vlassov S, Dorogin L, Butikova J, Smits K, Antsov M, Oras S, Zabels R and Lohmus R 2015 Metal nanodumbbells for nanomanipulations and tribological experiments *Phys. Scr.* **90** 094007
- [35] Korayem A H, Hoshier A K and Korayem M H 2015 Modeling and simulation of critical forces in the manipulation of cylindrical nanoparticles *Int. J. Adv. Manuf. Technol.* **79** 1505–17
- [36] Wang S, Hou L, Xie H and Huang H 2015 The kinetic friction between a nanowire and a flat substrate measured using nanomanipulation with optical microscopy *Appl. Phys. Lett.* **107** 103102
- [37] Polyakov B, Dorogin L M, Vlassov S, Kink I, Romanov A E and Lohmus R 2012 *In situ* measurement of the kinetic friction of ZnO nanowires inside a scanning electron microscope *Micron* **43** 1140–6
- [38] Clifford C A and Seah M P 2005 The determination of atomic force microscope cantilever spring constants via dimensional methods for nanomechanical analysis *Nanotechnology* **16** 1666–80
- [39] Cui J 2012 Zinc oxide nanowires *Mater. Charact.* **64** 43–52
- [40] Zhang Y, Ram M K, Stefanakos E K and Goswami D Y 2012 Synthesis, characterization, and applications of ZnO nanowires *J. Nanomater.* **2012** 1–22
- [41] Šutka A, Timusk M, Döbelin N, Pärna R, Visnapuu M, Joost U, Käämbre T, Kisand V, Saal K and Knite M 2015 A

- straightforward and ‘green’ solvothermal synthesis of Al doped zinc oxide plasmonic nanocrystals and piezoresistive elastomer nanocomposite *RSC Adv.* **5** 63846–52
- [42] Wang W, Wang L, Liu L, He C, Tan J and Liang Y 2012 Morphology-controlled synthesis and growth mechanism of ZnO nanostructures via the NaCl nonaqueous ionic liquid route *CrystEngComm* **14** 4997–5004
- [43] Song J, Wang X, Riedo E and Wang Z L 2005 Elastic property of vertically aligned nanowires *Nano Lett.* **5** 1954–8
- [44] Desai A V and Haque M A 2007 Mechanical properties of ZnO nanowires *Sensors Actuators A* **134** 169–76
- [45] Chen C, Shi Y, Zhang Y, Zhu J and Yan Y 2006 Size dependence of Young’s modulus in ZnO nanowires *Phys. Rev. Lett.* **96** 75505
- [46] Wen B, Sader J E and Boland J J 2008 Mechanical properties of ZnO nanowires *Phys. Rev. Lett.* **101** 2–5
- [47] Xu F, Qin Q, Mishra A, Gu Y and Zhu Y 2010 Mechanical properties of ZnO nanowires under different loading modes *Nano Res.* **280** 1–10
- [48] Stan G, Ciobanu C V, Parthangal P M and Cook R F 2007 Diameter-dependent radial and tangential elastic moduli of ZnO nanowires *Nano Lett.* **7** 3691–7
- [49] Polyakov B, Dorogin L M, Vlassov S, Kink I, Lohmus A, Romanov A E and Lohmus R 2011 Real-time measurements of sliding friction and elastic properties of ZnO nanowires inside a scanning electron microscope *Solid State Commun.* **151** 1244–7
- [50] Manoharan M P, Desai A V, Neely G and Haque M A 2008 Synthesis and elastic characterization of ZincOxide nanowires *J. Nanomater.* **2008** 1–7
- [51] Ni H and Li X 2006 Young’s modulus of ZnO nanobelts measured using atomic force microscopy and nanoindentation techniques *Nanotechnology* **17** 3591–7
- [52] Ji L-W, Young S-J, Fang T-H and Liu C-H 2007 Buckling characterization of vertical ZnO nanowires using nanoindentation *Appl. Phys. Lett.* **90** 033109
- [53] Agrawal R, Peng B, Gdoutos E E and Espinosa H D 2008 Elasticity size effects in ZnO nanowires—a combined experimental-computational approach *Nano Lett.* **8** 3668–74
- [54] Polyakov B, Antsov M, Vlassov S, Dorogin L M, Vahtrus M, Zabels R, Lange S and Lohmus R 2014 Mechanical properties of sol–gel derived SiO₂ nanotubes *Beilstein J. Nanotechnol.* **5** 1808–14
- [55] Zhang L and Huang H 2006 *Appl. Phys. Lett.* **89** 183111
- [56] Chen C Q, Shi Y, Zhang Y S, Zhu J and Yan Y J 2006 *Phys. Rev. Lett.* **96** 075505
- [57] Agrawal R, Peng B, Gdoutos E E and Espinosa H D 2008 *Nano Lett.* **8** 3668–74
- [58] Polyakov B, Vlassov S, Dorogin L M, Kulis P, Kink I and Lohmus R 2012 The effect of substrate roughness on the static friction of CuO nanowires *Surf. Sci.* **606** 1393–9
- [59] Vanossi A, Manini N, Urbakh M, Zapperi S and Tosatti E 2013 Colloquium: modeling friction: from nanoscale to mesoscale *Rev. Mod. Phys.* **85** 529–52
- [60] Liu Y and Szlufarska I 2012 Chemical origins of frictional aging *Phys. Rev. Lett.* **109** 186102
- [61] Smith D A, Holmberg V C and Korgel B A 2010 Flexible germanium nanowires: ideal strength, room temperature plasticity, and bendable semiconductor fabric *ACS Nano* **4** 2356–62
- [62] Ashby M F, Messler R W, Asthana R, Furlani E P, Smallman R E, Ngan A H W, Crawford R J and Mills N 2009 *Engineering Materials and Processes Desk Reference* (Waltham, MA: Butterworth-Heinemann)
- [63] Hirth J P and Lothe J 1982 *Theory of Dislocations* (New York: Wiley)
- [64] Hoffmann S *et al* 2006 Measurement of the bending strength of vapor–liquid–solid grown silicon nanowires *Nano Lett.* **6** 622–5
- [65] Lu C 2008 On the bending strength of ZnO nanowires *Phys. Lett. A* **372** 6113–5
- [66] Friedrich K 2012 *Application of Fracture Mechanics to Composite Materials* (Amsterdam: Elsevier) p 41
- [67] Feldmann M, Dietzel D, Fuchs H and Schirmeisen A 2014 Influence of contact aging on nanoparticle friction kinetics *Phys. Rev. Lett.* **112** 155503
- [68] Manoharan M P and Haque M A 2009 Role of adhesion in shear strength of nanowire–substrate interfaces *J. Phys. D: Appl. Phys.* **42** 095304
- [69] Yang S, Kooij E S, Poelsema B, Lohse D and Zandvliet H J W 2008 Correlation between geometry and nanobubble distribution on HOPG surface *Europhys. Lett.* **81** 64006
- [70] Bennewitz R, Gyalog T, Guggisberg M, Bammerlin M and Meyer E 1999 Atomic-scale stick-slip processes on Cu(111) *Phys. Rev. B* **60** 301–4
- [71] Gnecco E, Bennewitz R, Gyalog T, Loppacher C, Bammerlin M, Meyer E and Guntherodt H 2000 Velocity dependence of atomic friction *Phys. Rev. Lett.* **84** 1172–5
- [72] Braun O and Peyrard M 2011 Dependence of kinetic friction on velocity: master equation approach *Phys. Rev. E* **83** 046129-1-9